Investigating the effects of Silicon etching imperfections on the quadrature error in MEMS gyroscopes

Alexandre AZIER[1 2], Bernard CHAUMET[3], Najib KACEM[1], Noureddine BOUHADDI[1]

[1] Department of Applied Mechanics, FEMTO-ST, Besançon, France

[2] THALES AVS France SAS, Valence, France

[3] THALES AVS France SAS, Châtellerault, France

Abstract

In this paper we develop a new approach in order to understand the origin of the quadrature error in MEMS gyroscopes. In an ideal and symmetrical gyroscope, there would not be quadrature error. However, technological defects, such as dispersion in the etching of the flexure springs could be the source of non-zero stiffness coupling between the X-axis and the Y-axis. As the stiffness coupling can generate quadrature signal and as the width of the flexure springs is a critical parameter in the MEMS design, it is necessary to investigate the impact of the width dispersion on the stiffness coupling. To do so, we developed an approach which consists of determining the evolution of the stiffness matrix of the springs of the gyroscope as a function of the inhomogeneity of the bending beams width of the springs through FEA. A statistical analysis of the results of these simulations, allowed us to calculate the mean and the standard deviation of the absolute value of the amplitude of the quadrature signal for a given beam width dispersion. It turns out that even small silicon etching defects can generate high quadrature level with up to a root mean square (RMS) value of 1220 °/s for a bending beam width dispersion of 1%. Moreover, the quadrature error obtained through simulations has the same order of magnitude that the ones measured on the gyroscopes.

1. Introduction

Silicon MEMS are very attractive for many uses because of their miniaturization and their performances. Although these devices are already present in many everyday objects, such as smartphones, their use for navigation applications in space, aeronautics or autonomous vehicles remains a real scientific and technological challenge. Indeed, the technological advances made on MEMS have effectively made it possible to approach, without however achieving, the levels of precision sought for this type of application. As a matter of fact, in the world of high performance, MEMS sensors must be 10000 times more precise than consumer sensors. Thereby, it is very challenging to design and manufacture silicon MEMS gyroscopes with performance levels of tactical and navigation grades [1] [2], which are so far dedicated to Ring Laser Gyroscopes (RLGs) [3] [4], Fiber Optic Gyroscopes (FOGs) [4] [5] [6] and Hemispherical Ring Gyroscpes (HRGs) [7] [8].

Since the creation of first MEMS rate gyroscopes and accelerometers thanks to the work of miniaturization of inertial systems carried out by Draper Laboratory in the late 1980s [9] [10], the precision of MEMS gyroscopes has improved a lot in the last decades, from a bias of few hundred degrees per hour [9] [11], to few degrees per hour [12] [13] [14] [15]. Moreover, thanks to all these years of research in MEMS gyroscope mechanical design and to the unceasing improvements in microfabrication, silicon, high-quality packaging and electronics technology, MEMS gyroscopes with $0.1\,°/s$ bias and $0.01\,°/\sqrt{h}$ ARW (Angular Random Walk) are now a near reality [16] [17] [18] [19].

Vibrating gyroscopes consist of one or more mobile vibrating masses [17] [20] [21] connected to each other and to their support by bending beams (which act as springs) in order to constitute an excitation resonator and a detection resonator, the two being coupled to each other by the acceleration of Coriolis [22]. Thus, when the gyroscope rotates around its sensitive axis, the composition of the forced vibration with the angular rotation vector generates forces, thanks to the

Coriolis effect, which induces vibration of the moving masses in the sensitive axis. This vibration is then detected by a detection transducer, the electrical signals of which are exploited by an electronic circuit to deduce therefrom a value of the angular speed around the sensitive axis. Therefore, any parasitic force exerted on the resonator with the same frequency as the Coriolis force and in the same direction as the sensitive mode will results, if it is not compensated, in an error on the sensor output called bias or zero-rate output (ZRO) [23]. Even though the bias can be removed from the final output signal with calibration, it varies over time and is sensitive to temperature variations and external vibrations (this phenomenon is called bias instability). So, in practical cases, its absolute value is minimized in order to reduce its instability. To do so, it is necessary to identify the factors that contribute to the bias of the gyroscope.

One of the major error sources is the mechanical quadrature signal [23] [24] [25] [26]. The quadrature is an unwanted force resulting from the coupling stiffness between the excitation-mode displacement and the sensitive-mode of the gyroscope. This force has the same frequency as the Coriolis signal, but is in phase quadrature (90° phase shift) with it, hence its name [24] [27]. Although its amplitude can be far more important than the amplitude of the Coriolis signal, it is possible to set is impact on the output signal aside. Indeed, one can use the 90° phase shift between the Coriolis and the quadrature signal by using a phase sensitivity demodulation via a processing electronic. By doing so, it is possible to split the sense information in two, so we can retrieve the Coriolis output [28]. However, even a slight phase error on the demodulation ($< 1°$) can generate an important bias [29] [30] and the high amplitude of the Coriolis signal can saturate the input accepted by the demodulator [31]. It is then needed to reduce the amplitude of the quadrature signal.

One way to do so, is to cancel the quadrature motion of the resonator using sense feedback electrodes. This can be done by applying an electrostatic force to the sense combs, with the same amplitude and in phase opposition with the quadrature force [28] [32]. Else, the quadrature signal can be compensated before the sense signal being demodulated. One can do so by adding a compensation signal with the same amplitude and in phase opposition with the quadrature force via a dedicated close loop [33]. Both of these methods work properly, but their feedback needs to be modulated, still letting us with the phase error problem. To overcome this issue, dedicated correction combs can be used to cancel the mechanical coupling stiffness. The idea is to apply the right DC voltage on the correction combs, so the electrostatic stiffness of these combs has the exact opposite value of the mechanical coupling stiffness [27] [34] [35] [36] [37] [38].

Whatever the compensation method(s) chosen, it is important to design a well-balanced resonator, while taking into account the manufacturing defects [39]. Indeed, on most of the MEMS gyroscope design, one or several springs are place symmetrically on each corner of the resonator so, if all the springs are identical, the resulting coupling stiffness is null [30]. Yet, if there is geometrical dispersion of the flexure springs, especially width dispersion as it is a critical dimension for the springs, the resulting coupling stiffness would not be equal to zero, which would generate a quadrature force. To our knowledge, few investigations have been carried out about the contributions of the geometrical dispersion of the springs on quadrature error [27] [30] [40]. These, even though they point and demonstrate the importance of width dispersion for the quadrature error, don't make the link between width dispersion of the springs and the amplitude of the quadrature signal dispersion (i.e. the dispersion of the quadrature error of several gyroscope made with the same design).

Hence, in this paper, we present an approach to estimate the impact of silicon etching dispersion on the variation of the amplitude of the quadrature signal. To do so, we run simulations using a finite elements method (FEM) in order to estimate the evaluation of the stiffness matrix of the springs of the gyroscope. Then, we used these results in order to calculate statistical values of the quadrature error. Next, these values are compared to the measures of the quadrature error obtained using a dedicated bench.

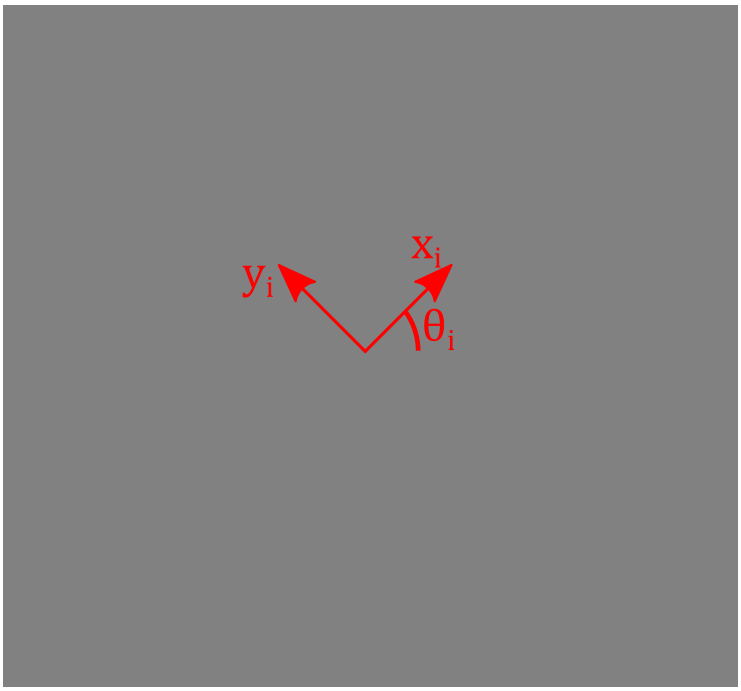

Fig. 1. Equivalent model of the gyroscope **[41]**

2. Gyroscope dynamics

The dynamic equations of a linear vibrating gyroscope can be expressed as [24] [42]:

$$\begin{bmatrix} m & 0 \\ 0 & m \end{bmatrix} \frac{d^2U}{dt^2} + ([D] + [C]) \frac{dU}{dt} + \begin{bmatrix} k_x & k_{xy} \\ k_{xy} & k_y \end{bmatrix} U = F \quad \textbf{(1)}$$

where m is the modal mass, $U = \begin{pmatrix} x \\ y \end{pmatrix}$ represents the displacement vector, $[D]$ represents the damping matrix, $[C] = \begin{bmatrix} 0 & -2m\Omega_z \\ 2m\Omega_z & 0 \end{bmatrix}$ represents the Coriolis matrix, Ω_z is the angular velocity around the z-axis, k_x and k_y represents respectively the stiffness along the x and y-axis, k_{xy} the coupling stiffness term bringing the quadrature signal and F the driving vector force. In the y-axis (the sensitive direction), the equation (1) becomes:

$$m\,\ddot{y} + d_y\dot{y} + k_y y = -k_{xy}x - 2m\Omega_z\dot{x} \quad \textbf{(2)}$$

It is then necessary to understand the origins and to calculate the k_{xy} term in order to deduce the amplitude of the quadrature signal. In this paper, we propose to evaluate the impact of silicon etching defaults on the coupling stiffness term.

3. Expression of the coupling stiffness

As we focus on the mechanical stiffness of the resonator, electrostatic combs are not taken into account in our study (their mass, though, are include in the total mass of the structure). That is why, for simplification purposes, an equivalent model of the considered gyroscope is used (cf. Fig. 1). In order to describe the stiffness matrix of the flexure springs, two coordinate systems are defined as follows:

- $B(\vec{x};\vec{y})$ is the canonical coordinate system (the x and y-axis)
- $B'_i(\vec{x_i};\vec{y_i})$ represents the eigenbase of the spring number i

Thus, the transition matrix P_i between B and B'_i is expressed by:

$$P_i = \begin{bmatrix} \cos(\theta_i) & -\sin(\theta_i) \\ \sin(\theta_i) & \cos(\theta_i) \end{bmatrix} \quad \textbf{(3)}$$

Moreover, we define $[k]_B^i$ and $[k]_{B'_i}^i$ the stiffness matrix of the i[th] spring wrote in the coordinate system B and B'_i respectively. Then, we have:

$$[k]_B^i = P[k]_B^i P^T \quad \textbf{(4)}$$

By substituting the equation (3) into the equation (4) we can deduce the total stiffness matrix $[K]_B$ of

the gyroscope, described in the B coordinate system:

$$[K]_B = \sum_{i=1}^{4n} [k]_B^i = \begin{bmatrix} K_x & K_{xy} \\ K_{xy} & K_y \end{bmatrix} \quad (5)$$

With:

$$K_x = \sum_{i=1}^{4n} k_x^i = \sum_{i=1}^{4n} \left(a_i + (-1)^i b_i \cos(2\theta_i)\right) \quad (6)$$

$$K_{xy} = \sum_{i=1}^{4n} k_{xy}^i = \sum_{i=1}^{4n} (-1)^i b_i \sin(2\theta_i) \quad (7)$$

$$K_y = \sum_{i=1}^{4n} k_y^i = \sum_{i=1}^{4n} \left(a_i - (-1)^i b_i \cos(2\theta_i)\right) \quad (8)$$

$$a_i = \frac{k_I^i + k_{II}^i}{2};\ b_i = \frac{k_I^i - k_{II}^i}{2} \quad (9)$$

Where k_I^i and k_{II}^i being the eigenvalues of the i[th] spring and $4n$ the total number of flexure springs.

Therefore, in order to calculate the value of the coupling stiffness, it is necessary to determine the evolution of k_x^i, k_y^i and k_{xy}^i with respect to the variation of the silicon etching imperfections, which can be done through FEM simulations.

A numerical three-dimensional finite element model has been developed on ANSYS™ to simulate the static mechanical response of the flexure springs. Our model consists of four Silicon springs, embedded on one end and subjected to a static load on the other end via a rigid remote point (cf. Fig. 2). The remote point coincides with the origin of the Cartesian coordinate system (x, y, z). The width dimensions, illustrated in Fig. 3, of each springs can be changed in a different manner for each springs, but the length l and the thickness h of the beams remain the same for all beams. This model was meshed using eight-node elements (HEX8). In total, up to 212000 elements and 276000 nodes were used. It should be noted that before carrying out simulations, a mesh sensitivity study was performed to ensure the convergence of the finite element simulation results. Degrees of freedom of the model's nodes are 3D displacements x, y and z.As we are keen to know the evolution of the coupling stiffness k_{xy} with respect to e_x and e_y, two steps of simulations are required.

For the first step, only the flexure springs 1 and 3 of the Fig. 2 are simulated and their widths are equal, i.e. $e_x = e_y = e_0$. In such geometrical configuration, springs 1 and 3 behave as pure linear spring when a load is applied along the X_1 and Y_1 axis. These axes correspond to the diagonals of the square shaped by the four beams of a flexure spring. Then, we can run two simulations, which simply consist of applying a load F on the remote point linked to the spring 1 and 3 along the T (respectively N) axis and retrieving the displacement d_T (respectively d_N) of the remote point along the same axis. So we have:

$$k_I^1 = k_I^3 = \frac{F}{2 * d_T} \quad (10)$$

$$k_{II}^1 = k_{II}^3 = \frac{F}{2 * d_N} \quad (11)$$

For the second step, all flexure springs represented in Fig. 2 are simulated, the widths of the spring 2, 3 and 4 are equal to e_0 (the same e_0 as in the first step) and the widths e_x and e_y of the spring 1 are not identical, i.e. $e_x \neq e_y$, but have a value close to e_0. Thereafter, we run two simulations, in which we set up a load F on the remote point connected to all the springs along the x (respectively y) axis and retrieving the displacement $\begin{pmatrix} X_1 \\ Y_1 \end{pmatrix}$ (respectively $\begin{pmatrix} X_2 \\ Y_2 \end{pmatrix}$) of the remote point along the x and y axes. Next, let $[S]$ denotes the stiffness matrix of our four springs-remote point system:

$$[S] = \begin{bmatrix} S_x & S_{xy} \\ S_{xy} & S_y \end{bmatrix} = \sum_{i=1}^{4} [k]_B^i \quad (12)$$

Thanks to the results of the previous simulations, we are able to calculate the terms of the matrix $[S]$:

$$S_x = \frac{F}{X_1}\left(1 + \frac{{Y_1}^2}{(Y_2X_1 - X_2Y_1)}\right) \quad (13)$$

$$S_{xy} = \frac{-FY_1}{(Y_2X_1 - X_2Y_1)} \quad (14)$$

$$S_y = \frac{FX_1}{(Y_2X_1 - X_2Y_1)} \quad (15)$$

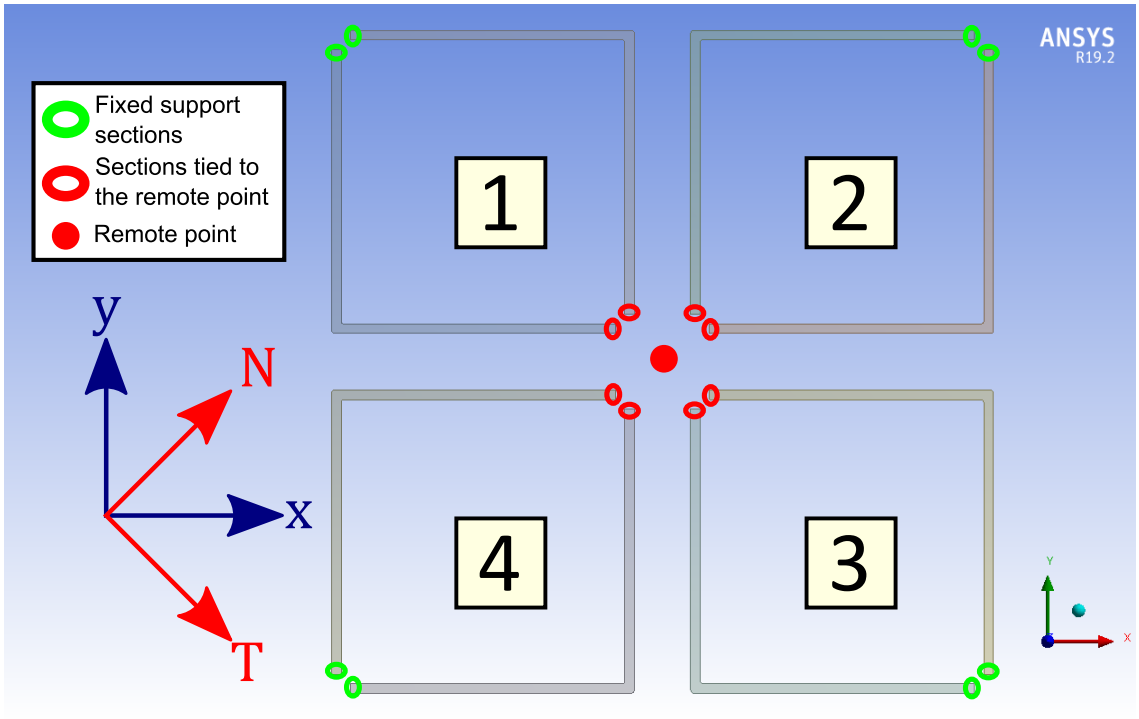

Fig. 2. Model used during simulations

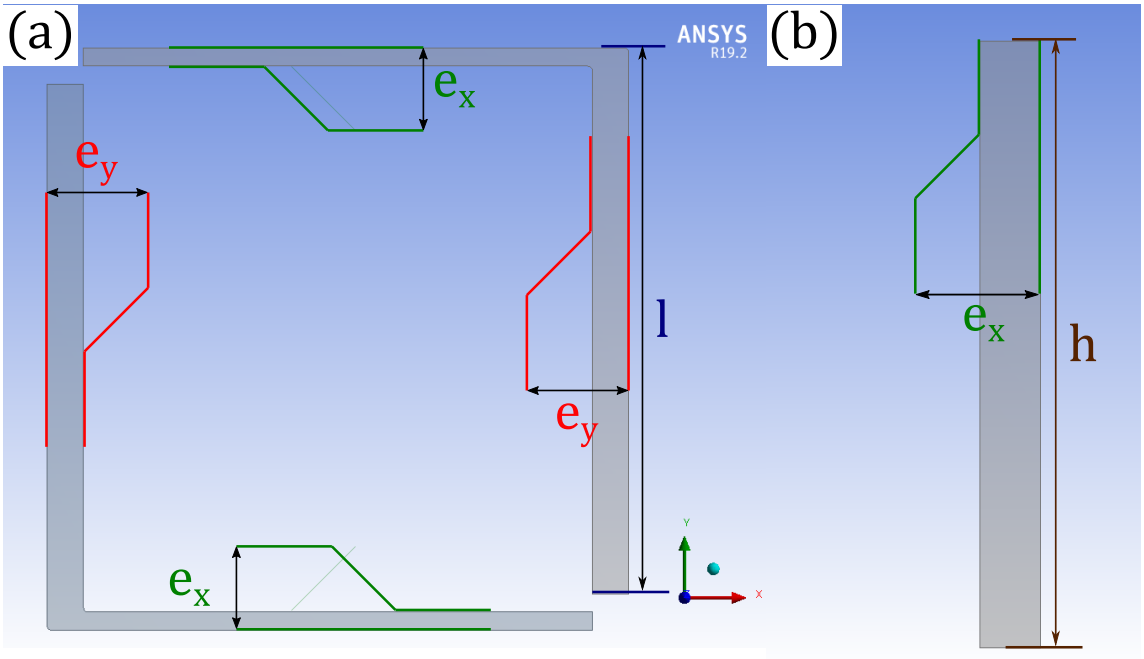

Fig. 3. Representation of the geometrical parameters of the spring 1 (a) View from XY plan (b) Cross section of one beam viwed from ZY plan

So, we are now able to calculate the value of $[k]_B^1$, the stiffness matrix of the spring 1, as we know the value of each terms of $[S]$ and of $[k]_B^i$ for the springs 2, 3 and 4 (thanks to the results obtained in the first step and to the equations (6) to (11)):

$$[k]_B^1 = [S] - \sum_{i=2}^{4} [k]_B^i \quad \textbf{(16)}$$

Then, we can run more simulations varying the value of e_x and e_y, (e_0 could also be changed if needed) while remaining in the permissible range of the silicon etching defaults.

Once we have done a certain number of finite element analysis by varying the widths the spring 1, we can determine the evolution of k_x^1, k_y^1 and k_{xy}^1 as a function of ε (Fig. 4), the value of the implemented geometric defects ($e_x = e_0 + \varepsilon$ and $e_y = e_0 - \varepsilon$). We also want to place emphasis on the fact that the evolution of the k_x and k_y terms as a function of ε is the same of the spring 1 to 4, only the evolution of the k_{xy} is different for the even-numbered and the odd-numbered spring $\left(k_{xy}^1(\varepsilon) = k_{xy}^3(\varepsilon) = -k_{xy}^2(\varepsilon) = -k_{xy}^4(\varepsilon)\right)$.

4. Impact on the amplitude of the quadrature signal

Knowing the evolution of k_x, k_y and k_{xy} versus the width error of the spring, we can perform statistical calculations. Indeed, the manufacturing process being not perfect, a different error is made of the width on each beam of each springs of the gyroscope. Here, we assume that this error follows a centered normal law $N(0\,;\,\varepsilon/3)$ for e_x and e_y, of each spring. So, based on the equation(4) (5) and the evolution formulas of k_x^i, k_y^i and k_{xy}^i versus the width error, 10^5 samples (a lot of samples are required in order to obtain accurate statistical values) are carried out, via a custom-built Matlab™ program, to calculate the mean and the standard deviation of the normalized amplitude of the quadrature signal KO_Q caused by the caused by the coupling stiffness (with ${\omega_0}^2 = \frac{{\omega_x}^2 + {\omega_y}^2}{2}$, $\omega_x = 2\pi\sqrt{\frac{K_x}{m}}$ and $\omega_y = 2\pi\sqrt{\frac{K_y}{m}}$).

$$KO_Q = \frac{K_{xy}}{2m\omega_0} \quad \textbf{(17)}$$

We can do so for different values of ε, in order to determine the evolution of the standard deviation of $|KO_Q|$ versus ε. Fig. 5 shows that really small inhomogeneity of the bending beams width can generate high quadrature level (up to a RMS value of 1220 °/s for $\varepsilon/e_0 = 1\%$).

Then, we can compare our model to the measurements.

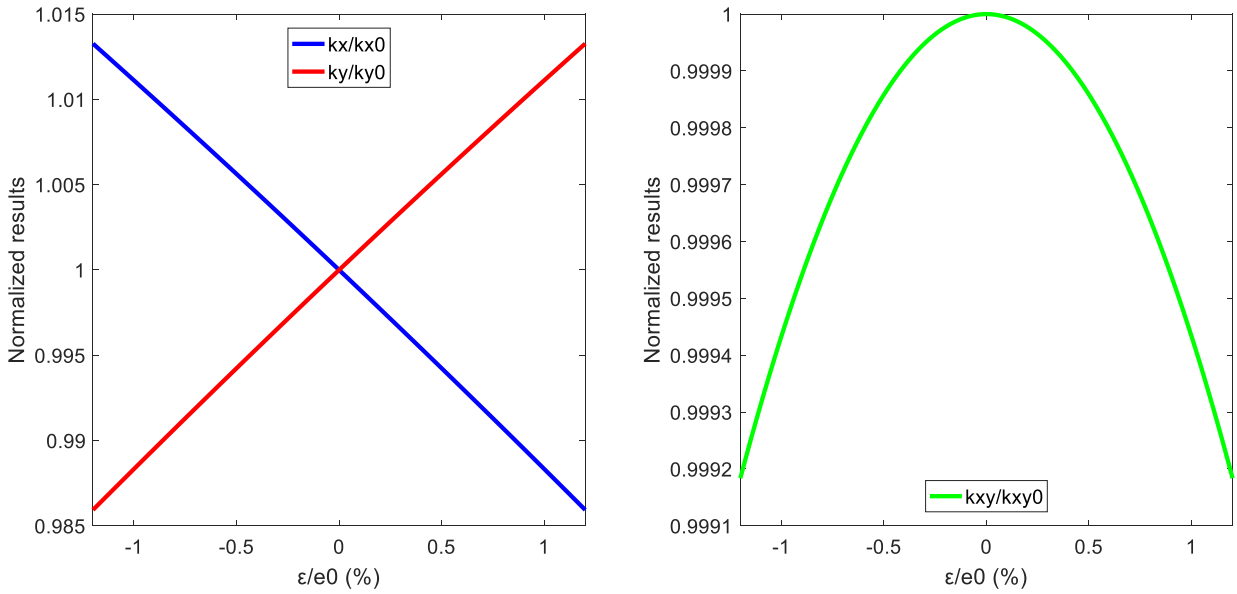

Fig. 4. Normalized $\mathbf{k_x^i}$, $\mathbf{k_y^i}$ and $\mathbf{k_{xy}^i}$ values as a function of the width error

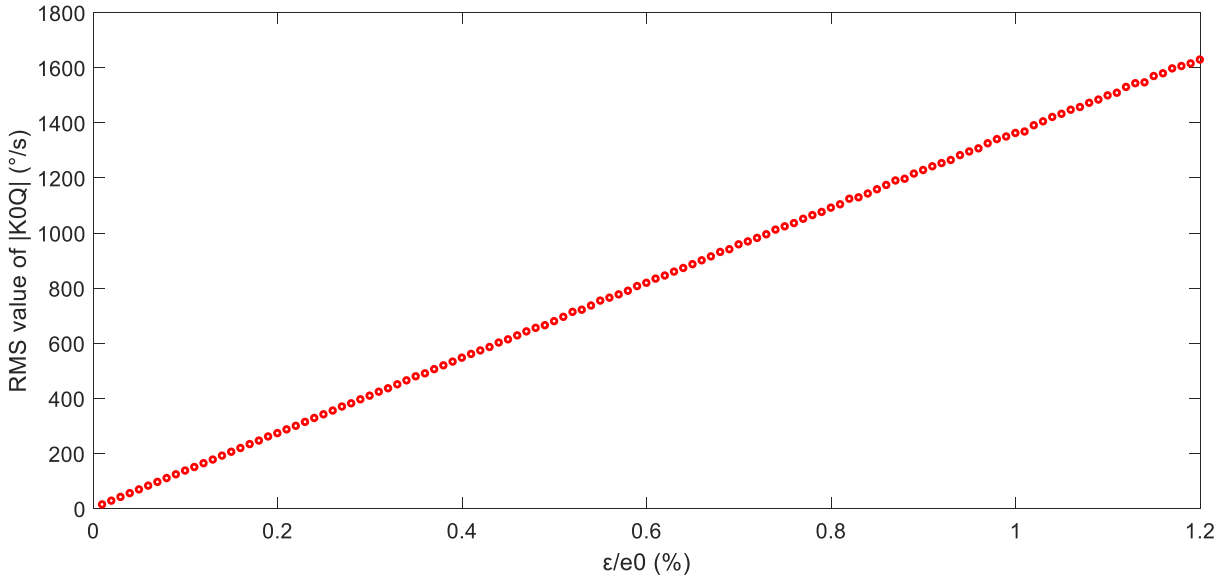

Fig. 5. RMS value of $|K0_Q|$versus standard deviation of the beam width error

5. Electrical measurements of the amplitude of the quadrature signal

5.1. Principle

As we work with high Q factor gyroscopes $(Q > 10^4)$ and low angular rate (vertical earth rotation), equation can be simplified as:

$$\begin{pmatrix}\ddot{x}\\ \ddot{y}\end{pmatrix} + \begin{bmatrix}{\omega_x}^2 & \frac{k_{xy}}{m}\\ \frac{k_{xy}}{m} & {\omega_y}^2\end{bmatrix}\begin{pmatrix}x\\ y\end{pmatrix} = \begin{pmatrix}0\\ 0\end{pmatrix} \quad \textbf{(18)}$$

If $\omega_x = \omega_y = \omega_0$, then equation (18) can be rewritten as:

$$\begin{pmatrix}\ddot{X}\\ \ddot{Y}\end{pmatrix} + \begin{bmatrix}{\omega_1}^2 & 0\\ 0 & {\omega_2}^2\end{bmatrix}\begin{pmatrix}X\\ Y\end{pmatrix} = \begin{pmatrix}0\\ 0\end{pmatrix} \quad \textbf{(19)}$$

Where:

- ${\omega_1}^2 = {\omega_0}^2 + \frac{k_{xy}}{m}$
- ${\omega_2}^2 = {\omega_0}^2 - \frac{k_{xy}}{m}$
- $x = \frac{X-Y}{2}$ and $y = \frac{X+Y}{2}$

Furthermore, if $\sqrt{\frac{k_{xy}}{m}} \ll \omega_0$, then :

$$(\omega_1 - \omega_2) \sim \frac{k_{xy}}{2m\omega_0} \quad \textbf{(20)}$$

Thus, according to equations (17) and (20), we have:

$$(\omega_1 - \omega_2) \sim KO_Q \quad \textbf{(21)}$$

Hence, if we are able to canceled the frequency mismatch (i.e. $\omega_x - \omega_y = 0$), we can estimate the amplitude of the quadrature signal by measuring ω_1 and ω_2.

5.2. Measuring bench

A dedicated bench, illustrated in Fig. 6, has been developed to measure the quadrature error of each cell. The cell is mounted on a homemade interface board allowed us to retrieve the electrical contacts with the electrodes of the gyroscope. The resonator contains combs ensuring multiple functions such as the frequency mismatch compensation, sense and drive [13] [16] [34]. A NI™ PXIe-1078 bench, with multiple modules and a custom-built LabVIEW™ program (cf. Fig. 7), was used to generate and record the excitation and detection signals. Each measurement was performed in three steps.

In the first step, we apply an appropriate DC voltage on the combs dedicated to the frequency mismatch compensation, in order to cancel the frequency difference between the X and Y-axis (i.e. $\omega_x - \omega_y \sim 0$). In the second step, a ring down test is performed: a DC voltage, generated by a generator, and a white noise voltage signal, filtered in a band close to the resonance frequency ω_0, is send by the PXI bench during two seconds (after

these two seconds the excitation is switched off), to the combs devoted to the drive function (both of these voltage pass through a custom-built filter to avoid any excitation noise). The PXI bench simultaneously records the decay of the resonator displacement via the sense combs (one set of combs for the x axis and another for the y axis) for a several seconds. Before being read by the PXI bench, the sense signals are amplified via a homemade charge amplifier, in order to convert the few nA of the transducer into dozens of mV. In the third step, our program filters the sense signals, in order to limit high and low frequency noise, and computes their power spectral density (PSD). Then, the program automatically find the maximum peaks of the PSDs and their frequency, which are the ω_1 and ω_2 frequencies of the equation (21).

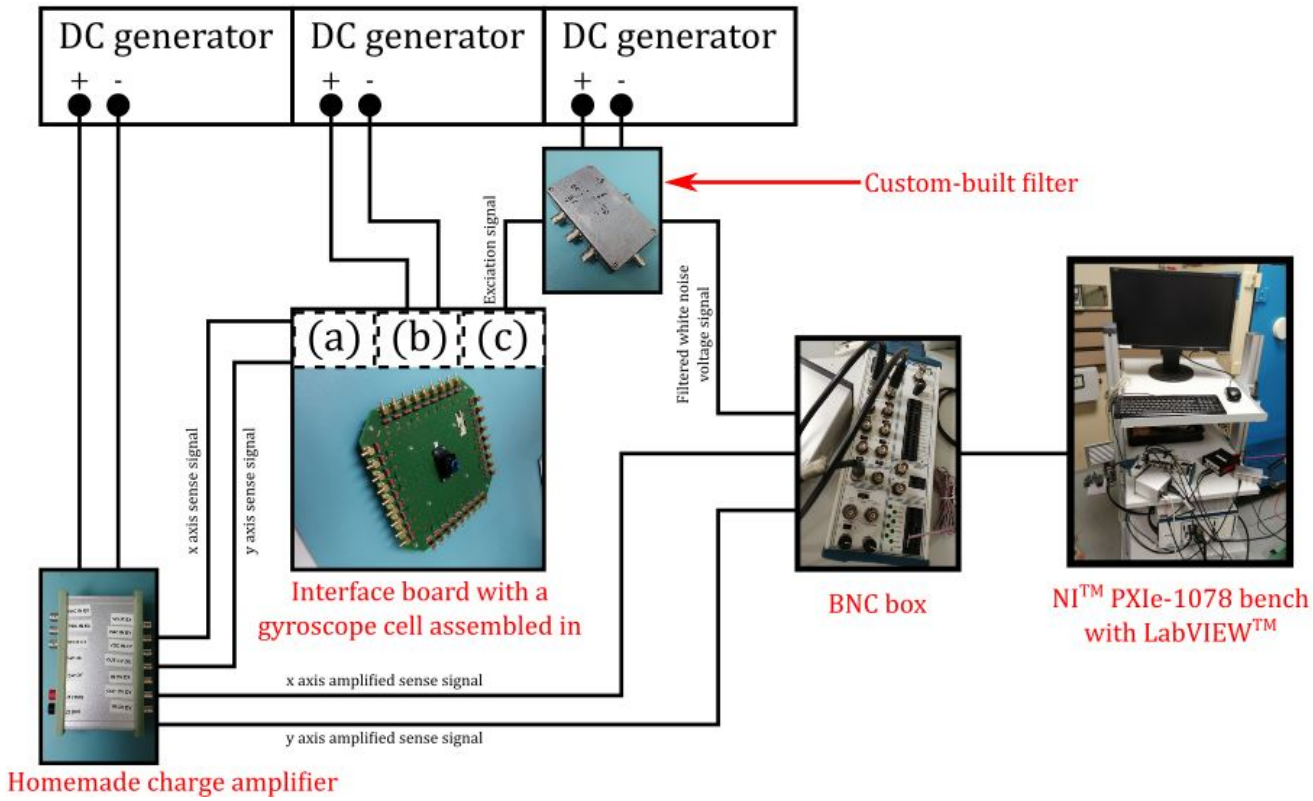

Fig. 6. Scheme of th bench developed to measure the quadrature error (a) Contact with the x axis and y axis sense electrodes (b) Contact with the frequency mismatch compensation electrodes (c) Contact with the x axis drive electrode(s)

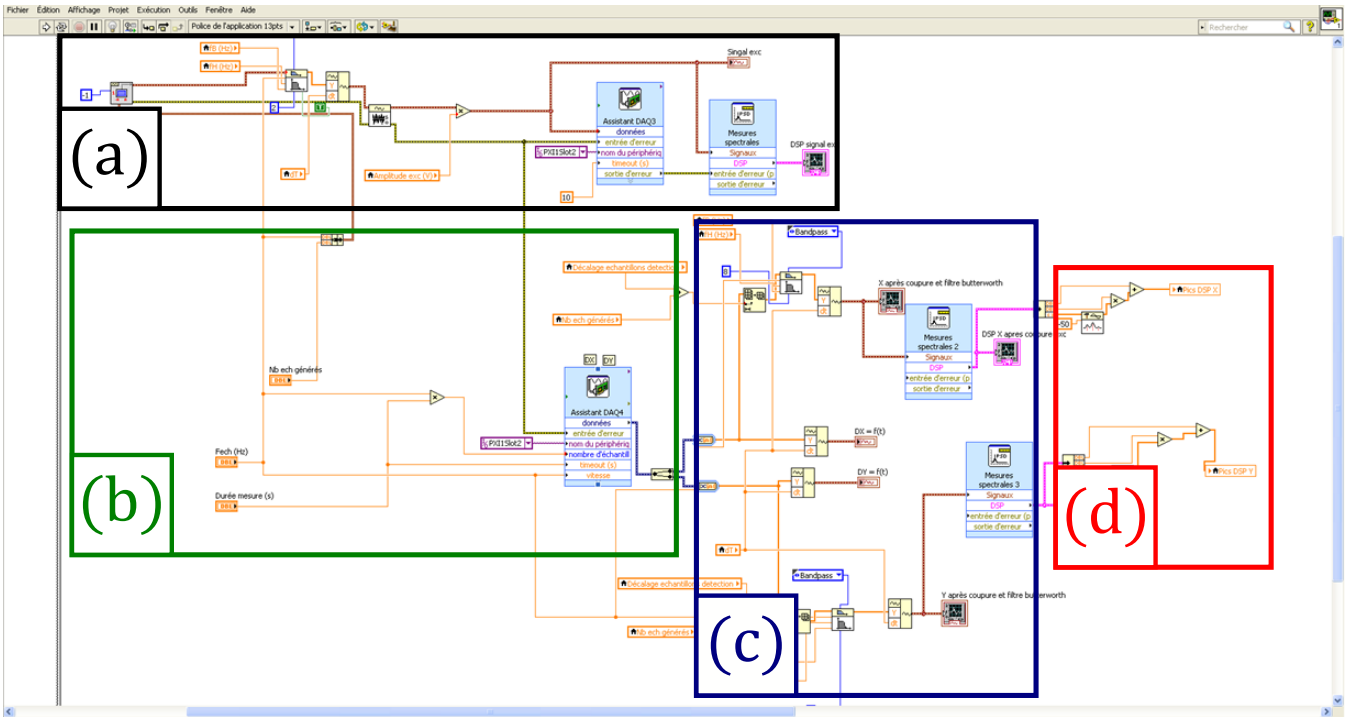

Fig. 7. View of the diagram of the LabVIEW™ program (a) Generation of the filtered white noise signal (b) Registration of the amplified x axis and y axis sense signals (c) Filtering the sense signals and computation of their PSD(d) Detection of the ω_1 and ω_2 frequencies

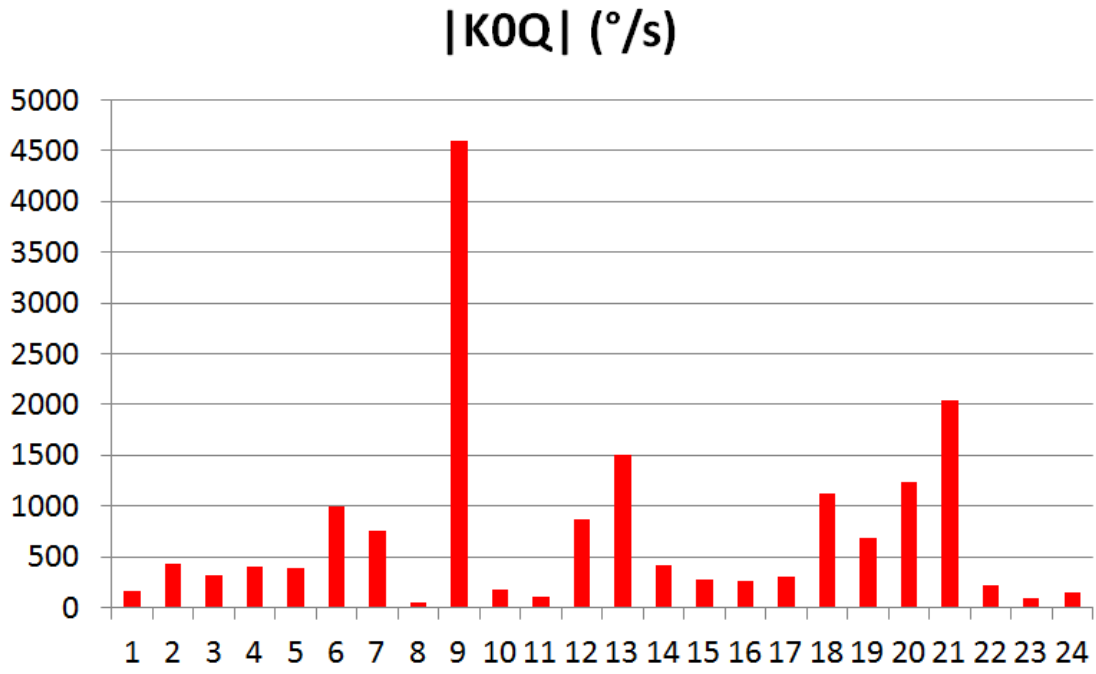

Fig. 8 $|K0_Q|$ measurements

5.3. *Experimental results*

The absolute value of the quadrature error was measured (one cannot tell the difference between the ω_1 peak and the ω_2 peak on the PSD) on a total of 24 cells and the results are shown in Fig. 8. A RMS value of 1210 °/s was calculated for the measurements of $|KO_Q|$, which is in the same order of magnitude as the results obtained through the numerical simulations (as mentioned in section 4).

That means that, for the next gyroscope design, it is necessary the take the bending beams width dispersion into account in order to avoid too many cells with high quadrature error.

It is important to notice that, even if our model match (for $\varepsilon/e_0 = 1\%$) with the measurements, it nevertheless does not mean that the inhomogeneity of the bending beams width is only cause of quadrature error. Indeed, this error may have many origins such as the design of the resonator, material anisotropy, broken springs, or any other geometrical inhomogeneity.

Conclusions

This paper provides an approach to evaluate the amplitude of the quadrature signal caused by an inhomogeneity of the bending beams width. It has been shown that such silicon etching defaults can generate high quadrature error, thus it is necessary to take them into account during the design of a MEMS gyroscope.

This is particularly true since high quality factor ($Q > 10^4$) resonators are essential levers to improve the performance and the sensitivity of MEMS gyro [43]. To achieve such high Q, it is necessary to reduce thermoelastic damping, which is one of the major energy losses in micromechanical resonators [44]. But to do so it is necessary to reduce the width of the bending beams of the vibrating system. However the inhomogeneity of the bending beams width, could then have a significant impact on the device performances (the ratio ε/e_0 would be increased). To overcome this issue, we can either reduce ε, i.e. the maximum dispersion of the bending beams width, or we can try to cancel the quadrature error. The first option requires to significantly improve the geometric accuracy of the etching technology, while the second option requires a specific architecture of the transducers and a control electronic [13] [27]. However, doing so might make the nonlinear regime of the resonators easily reachable, which could decrease the sensor performances [45]. Thereby, we need to find a compromise between the quadrature error cancelation and the nonlinear effects. Further research is underway to investigate the real inhomogeneity of the bending beams width via SEM observations of our resonator.

Acknowledgment

The authors would like to thank the engineers of the hardware department of Thales Avionics for their help for the calculations and the measures on the gyroscopes.

References

[1] J. Allen, "Micro-system inertial sensing technology overview," *Albuquerque, New Mexico,* 2009.

[2] Tronics, "An Overview of MEMS and non-MEMS gyros," *http://www.tronicsgroup.com,* 2013.

[3] P. Bouyer, "The centenary of Sagnac effect and its applications: From electromagnetic to matter waves," *Gyroscopy and Navigation,* vol. 5, no. 1, pp. 20-26, 2014.

[4] A. Shamir, "An overview of Optical Gyroscopes Theory, Practical Aspects, Applications and Future Trends," 2006.

[5] K. Grattan and T. Sun, "Fiber optic sensor technology: an overview," *Sensors and Actuators A: Physical,* vol. 82, no. 1-3, pp. 40-61, 2000.

[6] G. A. Sanders, S. J. Sanders, L. K. Strandjord, T. Qiu, J. Wu, M. Smiciklas, D. Mead, S. Mosor, A. Arrizon, W. Ho and others, "Fiber optic gyro development at Honeywell," in *International Society for Optics and Photonics*, 2016.

[7] D. M. Rozelle, "The hemispherical resonator gyro: From wineglass to the planets," 2009.

[8] F. Delhaye, "HRG by SAFRAN: The game-changing technology," in *IEEE*, 2018.

[9] J. Bernstein, S. Cho, A. King, A. Kourepenis, P. Maciel and M. Weinberg, "A micromachined comb-drive tuning fork rate gyroscope," in *IEEE*, 1993.

[10] M. S. Weinberg, "How to invent (or not invent) the first silicon MEMS gyroscope," in *IEEE*, 2015.

[11] G. N. Baker, "Quartz rate sensor from innovation to application," 1992.

[12] W. Geiger, J. Bartholomeyczik, U. Breng, W. Gutmann, M. Hafen, E. Handrich, M. Huber, A. Jackle, U. Kempfer, H. Kopmann and others, "MEMS IMU for ahrs applications," 2008.

[13] B. Chaumet, B. Leverrier, C. Rougeot and S. Bouyat, "A new silicon tuning fork gyroscope for aerospace applications," 2009.

[14] O. Deppe, G. Dorner, S. K{\"o}nig, T. Martin, S. Voigt and S. Zimmermann, "MEMS and FOG technologies for tactical and navigation grade inertial sensors—Recent improvements and comparison," *Sensors,* vol. 17, no. 3, p. 567, 2017.

[15] G. Wu, G. L. Chua and Y. Gu, "A dual-mass fully decoupled MEMS gyroscope with wide bandwidth and high linearity," *Sensors and Actuators A: Physical,* vol. 259, pp. 50-56, 2017.

[16] N. Vercier, B. Chaumet, B. Leverrier and S. Bouyat, "A new Silicon axisymmetric Gyroscope for Aerospace Applications," in *IEEE*, 2020.

[17] I. P. Prikhodko, S. A. Zotov, A. A. Trusov and A. M. Shkel, "Sub-degree-per-hour silicon MEMS rate sensor with 1 million Q-factor," in *IEEE*, 2011.

[18] S. Koenig, S. Rombach, W. Gutmann, A. Jaeckle, C. Weber, M. Ruf, D. Grolle and J. Rende, "Towards a navigation grade Si-MEMS gyroscope," in *IEEE*, 2019.

[19] D. Endean, K. Christ, P. Duffy, E. Freeman, M. Glenn, M. Gnerlich, B. Johnson and J. Weinmann, "Near-navigation grade tuning fork MEMS gyroscope," in *IEEE*, 2019.

[20] G. He and K. Najafi, "A single-crystal silicon vibrating ring gyroscope," in *IEEE*, 2002.

[21] A. A. Trusov, A. R. Schofield and A. M. Shkel, "Micromachined rate gyroscope architecture with ultra-high quality factor and improved mode ordering," *Sensors and Actuators A: Physical,* vol. 165, no. 1, pp. 26-34, 2011.

[22] W. Geiger, B. Folkmer, J. Merz, H. Sandmaier and W. Lang, "A new silicon rate gyroscope," *Sensors and Actuators A: Physical,* vol. 73, no. 1-2, pp. 45-51, 1999.

[23] N. Yazdi, F. Ayazi and K. Najafi, "Micromachined inertial sensors," *Proceedings of the IEEE,* vol. 86, no. 8, pp. 1640-1659, 1998.

[24] A. S. Phani, A. A. Seshia, M. Palaniapan, R. T. Howe and J. Yasaitis, "Modal coupling in micromechanical vibratory rate gyroscopes," *IEEE Sensors Journal,* vol. 6, no. 5, pp. 1144-1152, 2006.

[25] W. A. Clark, R. T. Howe and R. Horowitz, "Surface micromachined Z-axis vibratory rate gyroscope," 1996.

[26] H. Xie and G. K. Fedder, "Integrated microelectromechanical gyroscopes," *Journal of aerospace engineering,* vol. 16, no. 2, pp. 65-75, 2003.

[27] E. Tatar, S. E. Alper and T. Akin, "Quadrature-error compensation and corresponding effects on the performance of fully decoupled MEMS gyroscopes," *Journal of Microelectromechanical Systems,* vol. 21, no. 3, pp. 656-667, 2012.

[28] Y. Yin, S. Wang, C. Wang and B. Yang, "Structure-decoupled dual-mass MEMS gyroscope with self-adaptive closed-loop detection," in *IEEE*, 2010.

[29] M. Saukoski, L. Aaltonen and K. A. Halonen, "Zero-rate output and quadrature compensation in vibratory MEMS gyroscopes," *IEEE Sensors Journal,* vol. 7, no. 12, pp. 1639-1652, 2007.

[30] A. Walther, C. L. Blanc, N. Delorme, Y. Deimerly, R. Anciant and J. Willemin, "Bias contributions in a MEMS tuning fork gyroscope," *Journal of microelectromechanical systems,* vol. 22, no. 2, pp. 303-308, 2012.

[31] R. Antonello, R. Oboe, L. Prandi, C. Caminada and F. Biganzoli, "Open loop compensation of the quadrature error in MEMS vibrating gyroscopes," in *IEEE*, 2009.

[32] B. Y. Yeh and Y. C. Liang, "Modelling and compensation of quadrature error for silicon MEMS microgyroscope," in *IEEE*, 2001.

[33] J. Seeger, A. Rastegar and M. T. Tormey, *Method and apparatus for electronic cancellation of quadrature error,* Google Patents, 2007.

[34] B. Chaumet, F. Filhol, C. Rougeot and B. Leverrier, *MEMS angular inertial sensor operating in tuning fork mode,* Google Patents, 2017.

[35] C. C. Painter and A. M. Shkel, "Active structural error suppression in MEMS vibratory rate integrating gyroscopes," *IEEE Sensors Journal,* vol. 3, no. 5, pp. 595-606, 2003.

[36] J. Su, D. Xiao, X. Wu, Z. Hou and Z. Chen, "Improvement of bias stability for a micromachined gyroscope based on dynamic electrical balancing of coupling stiffness," *Journal of Micro/Nanolithography, MEMS, and MOEMS,* vol. 12, no. 3, p. 033008, 2013.

[37] B. J. Gallacher, J. Hedley, J. S. Burdess, A. J. Harris, A. Rickard and D. O. King, "Electrostatic correction of structural imperfections present in a microring gyroscope," *Journal of Microelectromechanical Systems,* vol. 14, no. 2, pp. 221-234, 2005.

[38] M. Maurer, T. Northemann and Y. Manoli, "Quadrature compensation for gyroscopes in electro-mechanical bandpass ΣΔ-modulators beyond full-scale limits using pattern recognition," *Procedia Engineering,* vol. 25, pp. 1589-1592, 2011.

[39] P. Merz, W. Pilz, F. Senger, K. Reimer, M. Grouchko, T. Pandhumsoporn, W. Bosch, A. Cofer and S. Lassig, "Impact of Si DRIE on vibratory MEMS gyroscope performance," in *IEEE*, 2007.

[40] S. V. Iyer, "Modeling and Simulation of Non-idealities in a Z-axis CMOS-MEMS Gyroscope," 2003.

[41] B. Chaumet, F. Filhol, C. Rougeot and B. Leverrier, "MEMS ANGULAR INERTIAL SENSOR OPERATING IN TUNING FORK MODE". Thales Avionics France Patent US 9,574,879 B2, 2015.

[42] V. Kempe, Inertial MEMS: principles and practice, Cambridge University Press, 2011.

[43] M. Weinberg, R. Candler, S. Chandorkar, J. Varsanik, T. Kenny and A. Duwel, "Energy loss in MEMS resonators and the impact on inertial and RF devices," in *IEEE*, 2009.

[44] T. V. Roszhart, "The effect of thermoelastic internal friction on the Q of micromachined silicon resonators," in *IEEE*, 1990.

[45] N. Kacem, S. Hentz, D. Pinto, B. Reig and V. Nguyen, "Nonlinear dynamics of nanomechanical beam resonators: improving the performance of NEMS-based sensors," *Nanotechnology,* vol. 20, no. 27, p. 275501, 2009.